Non-isothermal crystallization behavior of isotactic polypropylene/copper nanocomposites

J. M. Mata-Padilla[1,2] · C. A. Ávila-Orta[2] · A. Almendárez-Camarillo[3] · J. G. Martínez-Colunga[2] ·
E. Hernández-Hernández[2] · V. J. Cruz-Delgado[2] · P. González-Morones[2] · S. G. Solís-Rosales[2] ·
J. A. González-Calderón[4]

Abstract

The Non-isothermal crystallization behavior of isotactic polypropylene (iPP)/copper nanocomposites with four different mass percentages (0.5, 1.0, 2.0 and 4.0 mass%) of copper nanoparticles (nCu) were study by means of differential scanning calorimeter (DSC) at 2.5, 5, 10 and 20 °C min^{-1}. The nanostructure of PP/nCu nanocomposites was also studied by WAXD, SEM and optical microscopy, while their hierarchical crystalline morphologies (e.g., spherulites, lamellas and unit cell) were studied during the crystallization progress through polarized optical microscopy and in situ X-ray scattering at small and wide angle, observing that the spherulite size was not influenced by the nCu's, although the lamellas size and X-ray diffraction intensity increased with the incorporation of nanoparticles. The PP/nCu nanocomposites presented a mixture morphology with well-dispersed oxidized nanoparticles and some agglomerates, which were larger at higher concentration of particles. The crystallization results obtained by DSC indicated a displacement in the peak crystallization temperature at higher values. These results in combination with the kinetic of crystallization analyzed by the Jeziorny method clearly indicated an acceleration in the crystallization process. Additionally, the crystallization activation energy decreases for all nanoparticle's concentration, indicating a possible nucleating effect. However, the nucleation activity analyzed by the Dobreva and Gutzow's method showed that nCu could not be considered such as conventional heterogeneous nucleating agent of iPP. Conversely, the incorporation of nCu in the iPP matrix increased significantly the thermal conductivity of nanocomposites helping to the thermal dissipation from the melted macromolecules to the nCu's, accelerating the non-isothermal crystallization process.

Keywords Crystallization · Isotactic polypropylene · Copper nanoparticles · Nanocomposites · Nucleation activity · Thermal dissipation

Introduction

The polymer composites properties have been influenced by different factors such as component properties, composition, structure and interfacial interactions. These factors usually have been affected by the filler characteristics being the most important the particle size, size distribution, specific surface area and particle shape [1]. This behavior has been reported for micro- and nanoparticles and for different properties such as mechanical [2], thermophysical [2, 3], electrical [3]. For example, Zhang et al. [2] studied the effects of particle size and content on the thermal conductivity and mechanical properties of Al_2O_3/high-density polyethylene (HDPE) composites using four types of alumina particles with average diameters of 10, 4.7, 0.5 μm and 100 nm. The dispersion of the particles differs with particle size when the content is the

✉ J. M. Mata-Padilla
jose.mata@ciqa.edu.mx; jmmata@conacyt.mx

1   CONACyT-Centro de Investigación en Química Aplicada, Blvd. Enrique Reyna Hermosillo. 140, Col. San José de los Cerritos, CP 25294 Saltillo, Coahuila, Mexico

2   Centro de Investigación en Química Aplicada, Blvd. Enrique Reyna Hermosillo. 140, Col. San José de los Cerritos, CP 25294 Saltillo, Coahuila, Mexico

3   Departamento de Ingeniería Química, Tecnológico Nacional de México en Celaya, Av. Tecnológico y Antonio García Cubas s/n, 38010 Celaya, Guanajuato, Mexico

4   Departamento de Ingeniería Industrial, Tecnológico Nacional de México en Celaya, Av. Tecnológico y Antonio García Cubas s/n, 38010 Celaya, Guanajuato, Mexico

same. These authors observed that the alumina particle with smaller particle size can form thermal conductive alumina pathway more easily and has higher toughening efficiency for micrometric particles. However, nanoalumina particles can form aggregation and destroy the toughness. Additionally, they reported that in the tensile process, the size of voids decreases with the alumina particle size, thus alumina with smaller particle size can bring higher tensile strength. Similar results were reported by Kratochvíla et al. [3] for various aspects of electrical and thermophysical properties of nanocomposites based on low-density polyethylene matrix filled with nanostructuralized expanded graphite (EG) and standard, microsized graphite. These authors reported that the thermophysical properties of nanocomposites are higher than the neat matrix. However, the filler size and the aspect ratio affect the heat propagation in the composite and the thermophysical behavior. Besides, they showed that the filler size affects also the electrical behavior and the electrical percolation threshold. The percolation concentration of the filler in nanocomposites filled with EG of large sizes was significantly lower than for the smaller ones that are more able for creation of aggregate. Additionally, the particle size has been also affected the nucleation and crystallization of semicrystalline polymers such as polypropylene, being the effect more prominent when it was introduced nanoparticles than agglomerates of this nanoparticles into the polymer matrix due to their higher surface area [4].

Although it is clear the advantage to use nanoparticles as filler of polymers in order to increase thermophysical, mechanical and electrical, the maximization of these properties in polymer nanocomposites could be achieved when the nanoparticles are deagglomerated and well distributed or dispersed into the polymer matrix. A methodology which has been successful for solving this problem is the direct application of ultrasound waves during melt blending in an extrusion process [5–9]. Likewise, the main advantage of the latter method is that it can be performed under solvent-free conditions.

On the other hand, in recent years has been increased the scientific and technological interest on the nanocomposites based on polypropylene and metal nanoparticles (e.g., copper, silver, gold, aluminum, etc.) due to their different properties such as antimicrobial, mechanical, thermal, electrical and electromagnetic agents [10–13]. Particularly, the nanocomposites of isotactic polypropylene (iPP) with copper nanoparticles (nCu) have been recently studied due to the efficiency of nCu to enhance the antimicrobial, electrical and electromagnetic properties of the PP matrix [14–17]. For example, España-Sánchez et al. [15] developed argon surface plasma treatment (APT) of poly(propylene)/silver (PP/Ag) and poly(propylene)/copper (PP/Cu) nanocomposite improving their antibacterial properties against pathogenic bacteria (*S. aureus* and *P. aeruginosa*). These authors found that the antibacterial activity of PP/Cu nanocomposites were more effective than PP/Ag nanocomposites.

It has been reported by our group and other researchers that the intrinsic properties of semicrystalline polymer material are highly dependent on the hierarchical microstructure (e.g., spherulites, lamellas and crystalline structures) of the final products [8, 18–21]. These microstructures are function of the thermal or mechanical history that the material experiences during processing. Due to the practical processes usually proceed under non-isothermal crystallization conditions, it is useful to study the non-isothermal crystallization kinetics of PP/nCu nanocomposites. The investigation of non-isothermal crystallization kinetic of polymers has significant relevance from the theoretical and practical point of view. The theoretical analysis has been associated with the mechanism of formation of the polymer structure during crystallization, while the practical topic arises from the crystallinity grade on the physical and chemical properties of polymers [22].

Conversely, the crystallization kinetic of polypropylene nanocomposites has been influenced by the heterogeneous nucleation effect of different nanoparticles [23–28] and/or by the thermal conductivity of the nanofiller, which helped to increase the heat dissipation of polymer nanocomposites during the exothermic event (crystallization) [29, 30]. Radhakrishnan et al. determined the effect of thermal conductivity of different fillers such as wollastonite, glass fiber, silica, talc, mica, calcium carbonate and carbon fiber on the crystallization, structure, and morphology of iPP, determining that the degree of crystallinity of the polymer decreased with an increase in thermal conductivity and cooling rate, while the induction time and half time of crystallization decrease with the thermal conductivity of fillers.

Nonetheless, there is not enough knowledge about the effect of metal nanoparticles with high thermal conductivity, such as nCu, on the non-isothermal crystallization kinetic and activation energy of isotactic polypropylene (iPP). Additionally, it is important to determine whether the crystallization behavior of these nanocomposites could be associated with the nucleation activity or with the thermal conductivity of nanoparticles. In this sense, the aim of present study is to contribute to the comprehension of the overall non-isothermal crystallization of iPP/nCu nanocomposites under different concentrations of nanoparticles (i.e., 0.1, 0.5, 1.0, 2.0 and 4.0 mass%) and different crystallization rates (2.5, 5.0, 10.0 and 20.0 K min^{-1}) and determine the possible influence of the thermal conductivity of the copper nanoparticle on the crystallization phenomena. The nanocomposite morphology, the crystallization kinetics, the activation energy and crystalline morphology of the PP/nCu nanocomposites were also studied. This study is important from the point of view of the possible relationship between heat conductivity applications and the effect of this property on the non-isothermal

crystallization of polypropylene nanocomposites with highly thermal conductive particles such as copper nanoparticles.

Experimental

Materials

The iPP sample used in this study had a number-average molecular of 50,000 g gmol^{-1} and mass-average molecular masses of 190,000 g gmol^{-1}. The iPP was purchased from Aldrich (USA). Copper nanoparticles partially passivated (nCu) with a spherical morphology of 25 nm (diameter) and purity of 99.8% were supplied by SkySpring Nanomaterials, Inc. (USA).

Preparation of iPP/nCu nanocomposites

PP/nCu's composites were obtained by melt extrusion (463 K, 30 rpm), using a low shear configuration single screw extruder ($D = 3.07$ cm) with L/D ratio $= 12$, assisted by catenoidal ultrasonic horn from Branson Ultrasonics Corp., CT ($D = 1.27$ cm) which were connected to a homemade ultrasonic generator (35 kHz $\pm$ 1 kHz, 60% of 750 W), with 0.5, 1.0, 2.0, 4.0 mass% of nCu's. A scheme of this system was previously reported [8]. The same treatment was done for the neat PP sample (PP-US).

Scanning electron microscopy (SEM)

SEM observations were used to determine the dispersion of nCu's in the PP/nCu nanocomposites and to determine the nanostructure of PP/nCu nanocomposites. Pieces of injection molded probe of PP/nCu nanocomposite were cryo-fractured and coated with gold/palladium previously, for the dispersion determination. SEM micrographs were obtained using a field emission scanning electron microscope JSM-74101F-JEOLVR. A SEI detector with a voltage of 4.0 kV was used.

X-ray diffraction (WAXD)

A Siemens D-50 diffractometer was used to collect the corresponding X-ray diffraction patterns. The diffraction patterns of the PP-US and PP/nCu nanocomposites were obtained within the 2θ range 5°–80° using a scanning rate of 0.3° min^{-1}, a filament intensity of 25 mA and an accelerating voltage of 35 kV.

Optical microscopy

Optical microscopy (OM) observations were used firstly to determine the dispersion of PP/NCu composites at different

nCu's mass percentages (0.1, 0.5, and 1.0 mass%) prepared through melt extrusion process with and without ultrasound assistance. The dispersion was evaluated in terms of the area ratio (A_{ratio}) and mean diameter (D_m) on different samples. Image Pro Plus software from Media Cybernetics was used to analyze the images. OM observations, using the cross-polarized, were also realized on a cut (20 mm) of injection molding probe of PP/nCu nanocomposite with 0.1 mass% of nanoparticles to determine its crystalline morphology. Also, the OM in light polarized mode (POM) was used to observe the spherulite morphology of iPP and iPP/nCu nanocomposite after the non-isothermal crystallization at 2.5 K min^{-1}. POM observations were performed in an optical microscope Olympus BX53 (Tokyo, Japan).

Differential scanning calorimetry (DSC)

Thermal experiments were made in a TA Instruments Model DSCQ2000 differential scanning calorimeter (DSC). The equipment was calibrated with Indium standard using a constant nitrogen flow both in the sample and in the reference chambers. All samples weighted 8 ± 1 mg and were sealed within aluminum pans before positioning them in the sample holder. In the non-isothermal crystallization experiments, samples were heated up to 463 K for 5 min to and then they were cooled down to 298 K, at four different rates (2.5, 5.0, 10 and 20 K min^{-1}).

In situ small and wide-angle x-ray scattering (SWAXS)

In situ SWAXS crystallization measurements of PP-US and PP/0.5 mass%nCu samples were performed using a SAX-Sess mc2 (Anton-Paar, Graz, Austria). An X-ray generator with a long fine focus sealed glass X-ray tube (GE) was operated at 40 kV and 50 mA. A focusing multilayer optics and a block collimator provided an intense monochromatic primary beam (Cu-Ka, $\lambda = 0.1542$ nm). The samples were filled into a sample holder for solids. The sample holder was placed into a TCS-130 temperature-controlled sample holder unit (Anton-Paar) along the line shaped X-ray beam in the evacuated camera. The samples were cooled from 190 to 100 °C, at 2.5 K min^{-1}. The SWAXS-2D patterns were collected at different temperatures (463, 423, 408, 403, 398, 393, 383 and 373 K). The 2D-scattered intensity distribution was collected on an imaging-plate (IP) detector, and it was after reading out by a Cyclone storage phosphor system (Perkin Elmer, USA). 2D data were integrated into the one dimensional in the SAXS Quant 2D 3.91 software. The background scattering contributions were corrected, and the desmearing correction was also done.

Thermal diffusivity analysis

The measurements of thermal diffusivity (α) of PP/nCu nanocomposites were performed by means of diffusivity thermal analyzer Discovery Xenon Flash (DXF-200) from TA Instruments, USA. Disk probes ($D = 1.25$ cm, thickness ≈ 2 mm) were used for the measurements, and they were previously weighed (w) to obtain the density for each sample in study ($\rho = w/V$). All samples were also coated with graphite to increase their emissivity and reduce their transparency. The measurements were taken at 298 ± 2 K with a Xenon pulse of 500 µs. The values reported were the average of three-time measurements. The thermal conductivity was determined by the equation $k = C_p \alpha \rho$. The value of C_p used in this work was 1757 kJ kg^{-1} K^{-1}.

Results and discussion

Morphology of iPP/nCu nanocomposites

Figure 1 displays the elemental analysis performed by EDX mapping micrographs for the nanocomposites of polypropylene with the different mass percentages of copper nanoparticles (nCu). This figure shows green dots related to the copper nanoparticles which increased their content with the nanoparticle mass concentration. Additionally, there are some agglomerated particles (see arrows) in all nanocomposites. The agglomeration measurements are presented in Fig. 3 and Table 1.

On the other hand, in Fig. 2, the WAXD patterns for all iPP nanocomposite samples are presented. This figure shows the characteristic crystalline planes of Cu^0 ([111], [200] and [220]), represented in Fig. 2a; however, it is also observed the crystalline planes of Cu$_2$O ([110], [111], [200] and [220]), indicating that the copper nanoparticles were
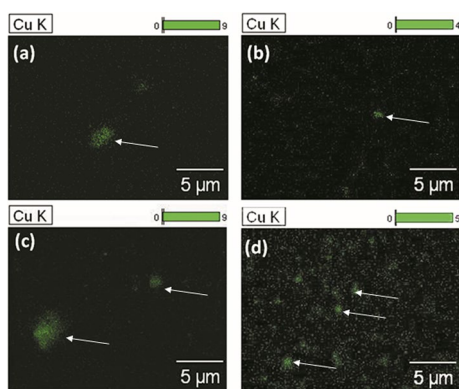

Fig. 1 EDX mapping micrographs of iPP nanocomposites with different mass percentages of nCu: **a** 0.5 mass%, **b** 1.0 mass%, **c** 2.0 mass% and **d** 4.0 mass%

Table 1 Area ratio (A_{ratio}) and mean diameter (D_{m}) of PP/nCu nanocomposites with different concentrations of nanoparticles

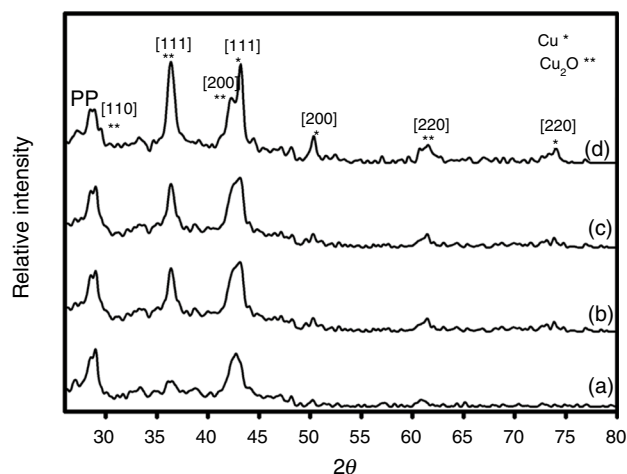| Sample	A_C/A_T/%	D_m/µm
PP/0.5 mass%nCu	0.32 (± 0.04)	9.10 (± 1.44)
PP/1.0 mass%nCu	0.53 (± 0.21)	9.36 (± 2.52)
PP/2.0 mass%nCu	1.48 (± 0.62)	11.78 (± 1.05)
PP/4.0 mass%nCu	5.06 (± 2.95)	16.41 (± 2.39)

Fig. 2 WAXD patterns of iPP nanocomposites, showing the copper nanoparticles region, with different mass percentages of nCu: (a) 0.5 mass%, (b) 1.0 mass%, (c) 2.0 mass% and (d) 4.0 mass%

partially oxidized during the nanocomposites processing. This behavior has been before reported by Hwang et al. [31]. These authors demonstrated that when the copper nanoparticles were exposed to the ambient, the surface of NPs were first oxidized forming a copper oxide I (Cu$_2$O) and after then it is transformed in copper oxide II (CuO).

Figure 3 shows OM micrographs of iPP/nCu samples with the different mass percentages (0.5, 1.0, 2.0 and 4.0 mass%) of nanoparticles prepared with ultrasound assistance. This figure clearly shows the presence of well-dispersed small agglomerates at low concentration of nanoparticles (0.5 and 1.0 mass%) due to the ultrasonic treatment. Conversely, the dispersion grade decreased at higher contents of nanoparticles (2.0 and 4.0 mass%), and the clusters size increased. The (A_{ratio}) and mean diameter (D_{m}) were determined using at least six OM micrographs for nanocomposites with 0.5, 1.0, 2.0 and 4.0% of nCu (see Table 1). The $A_{\mathrm{ratio}} = A_c/A_T$, where A_c is the area of nCu agglomerates and A_T is the whole area captured. The data in Table 1 probed that the area (0.32 and 0.53) and the mean diameter (9.10 and 9.33 mm) of nCu agglomerates are practically equal for the 0.5 and 1.0 mass% nCu nanocomposites, and these parameters increased significantly at the highest concentration (4.0 mass%).
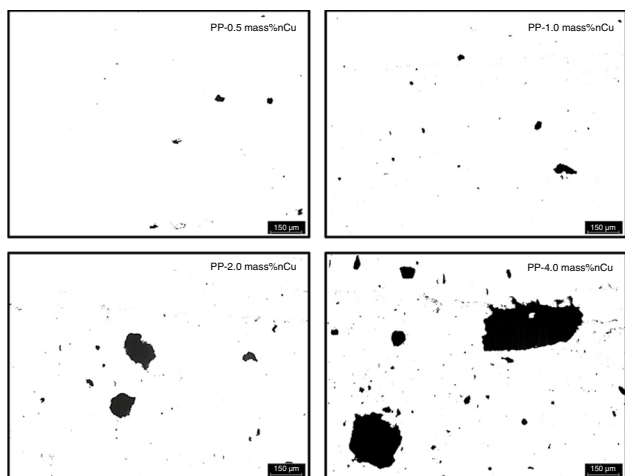
Fig. 3 Optical micrographs of PP/nCu nanocomposites with different concentrations of nCu (0.5, 1.0, 2.0 and 4.0 mass%)

Non-isothermal crystallization of iPP/nCu nanocomposites

Non-isothermal crystallization behavior of iPP and the iPP/nCu nanocomposites with different concentrations of nanoparticles (0.5, 1.0, 2.0 and 4.0 mass%) was studied by DSC at different cooling rates (2.5, 5, 10 and 20 K min^{-1}). The exothermal curves for all samples at the different cooling rates ϕ are shown in Fig. 4. The temperature of crystallization at peak (T_p) for the iPP at 2.5 K was 395.8 K, and it increased at 398 K for the iPP/NCu nanocomposites for the different nanoparticle concentrations. Similar behavior was observed for the curves at the different cooling rates, being the highest T_p value displacement respect to the iPP sample for the crystallization at 20 K min^{-1} of iPP/nCu samples with 0.5 and 1.0 mass% of nCu (≈ 4.0 °C) (see Table 2). Last behavior has been previously reported in the literature for polypropylene nanocomposites with different type of metal
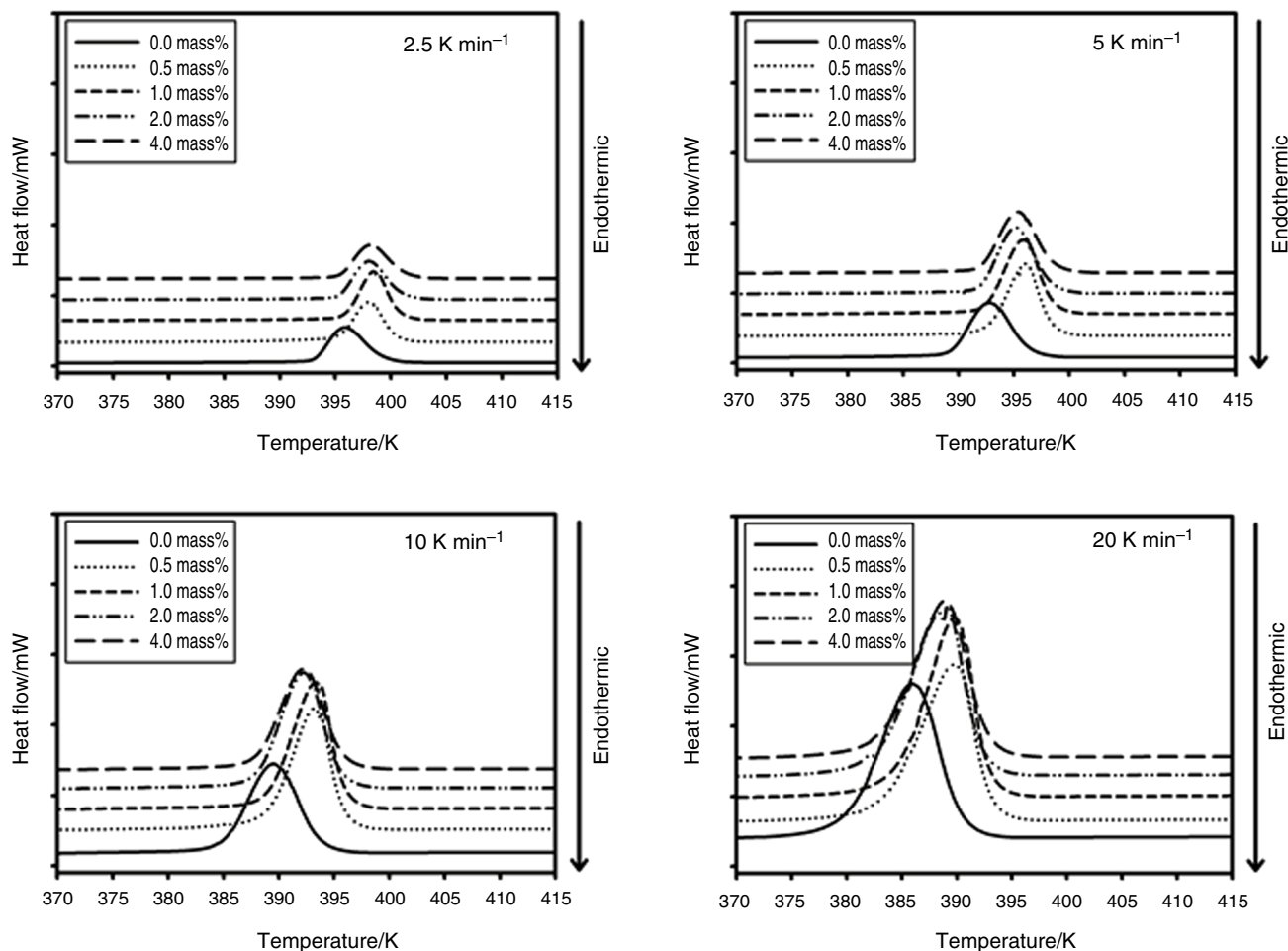

Fig. 4 DSC cooling traces for the iPP and iPP/nCu nanocomposites samples with diverse nCu concentrations (0.0, 0.5, 1.0, 2.0 and 4.0 mass%) at different cooling rates (2.5, 5, 10 and 20 K min^{-1})

Table 2 Crystallization temperature at peak (T_p) and overall crystallization time (t_c) of PP-US and PP/nCu nanocomposites with the different nanoparticle mass % and at different crystallization rates (ϕ)

Sample	2.5 K min⁻¹		5 K min⁻¹		10 K min⁻¹		20 K min⁻¹	
	T_p/K	t_c/min	T_p/K	t_c/min	T_p/K	t_c/min	T_p/K	t_c/min
PP-US	395.8	10.92	392.8	5.24	389.5	1.75	385.9	1.26
PP/0.5 mass%nCu	398.0	11.00	396.1	5.3	393.3	2.38	389.8	1.38
PP/1.0 mass%nCu	398.4	11.00	395.9	4.92	393.4	2.36	389.9	1.16
PP/2.0 mass%nCu	398.1	10.64	395.3	4.82	392.2	2.46	389.1	1.32
PP/4.0 mass%nCu	398.1	11.6	395.5	5.24	392.2	2.54	388.9	1.22

nanoparticles like as silver [32] and gold [33], obtaining similar results about the shifting in the crystallization temperature (≈ 3 K). This behavior has been associated with the nucleation effect of metal nanoparticles on the iPP matrix; however, this possible effect will be widely discussed after in next sections. Additionally, Table 2 also shows the overall crystallization time (t_c) for all studied samples. These results indicated that the values of t_c did not changed significantly in the iPP/nCu nanocomposites with respect to the iPP-US sample for all crystallization rates.

Non-isothermal crystallization morphological analysis

In situ non-isothermal crystallization WAXS and SAXS measurements were realized at specific temperatures (408, 403, 398, 393 and 383 K), according to the DSC cooling traces at 2.5 K min⁻¹, in order to investigate the effect of nCu incorporation in the crystalline and lamellar structures of polypropylene. Figure 5a shows that the T_p of polypropylene was displaced to higher temperature when the nCu's were incorporated. The WAXS results, as shown in Fig. 5b, indicate that around the induction temperature of crystallization (≈ 408 K) the PP-US sample present a more intense WAXS
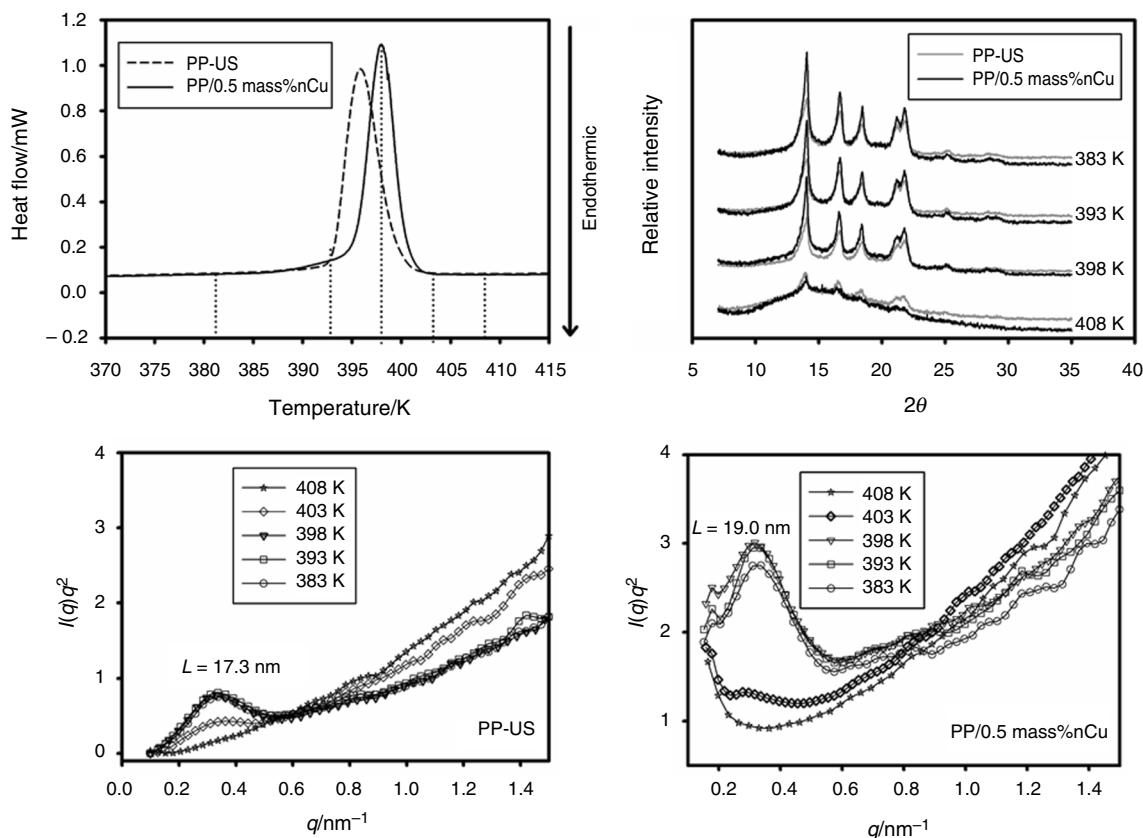

Fig. 5 In situ WAXS (**b**) and Lorentz-corrected SAXS (**c, d**) morphological analysis realized during the non-isothermal crystallization event, according to the DSC traces (**a**) at 2.5 K min⁻¹ for the PP-US and PP/0.5 mass%nCu nanocomposite

pattern than the PP/0.5 mass%nCu sample which could indicate that the crystallization of pristine PP macromolecules begun at lightly higher temperature than the PP nanocomposite. Conversely, when the crystallization progress, it was observed a higher increase in the crystalline reflections of PP nanocomposite sample than in the PP-US sample, indicating that the incorporation of copper nanoparticles helped to develop higher crystalline PP structures. It can be also seen that the characteristic reflections of the α crystalline habit of iPP were not modified by the nCu presence. Similar behavior was reported by Fanegas et al. [34], when nucleating agents (methylene-bis-(4,6-di-tertbutylphenyl) phosphate sodium salt) were incorporated in PP and PP blends matrices.

The Lorentz-corrected SAXS patterns of PP-US and PP/0.5 mass%nCu samples are displayed in Fig. 5c, d, respectively. The progress of crystallization indicated that at the temperature of 403 K, the long period SAXS peak growth at the position of 0.35 nm^{-1} practically not changed at lower temperatures. The average long period (L) was determined by the SAXS peak maxima by $L = \frac{2\pi}{q}$ [=]nm. The L value obtained for the PP-US sample was 17.3 nm. On the other hand, the PP/0.5 mass%nCu sample first develops a SAXS peak at $q \approx 0.28$ nm^{-1} ($L \approx 22.0$ nm) for the temperature of 408 K; however, when the crystallization phenomena progressed the SAXS patterns were displaced to lower q values. The q value obtained for the SAXS pattern at 373 K was 0.33 nm^{-1} which corresponds to a L value of ≈ 19 nm. An increase in long period thickness of non-isothermally crystallized nucleated iPP was previously observed by Fanegas et al. [34].

In the case of this work, we could infer that the incorporation of nCu in the iPP matrix generated wider and more imperfect lamellar crystals [35]. Nonetheless, the complete explanation about this behavior will be studied in a future work.

The influence nCu on the microscopic morphology (spherulites) of the iPP, after the non-isothermal crystallization at 2.5 K min^{-1}, was investigated by polarized optical microscopy (POM). The POM micrographs are shown in Fig. 6. This figure showed that the PP spherulite morphology was not highly influenced by the incorporation of nCu in terms of crystal size, although the spherulites of PP/0.5 mass%nCu
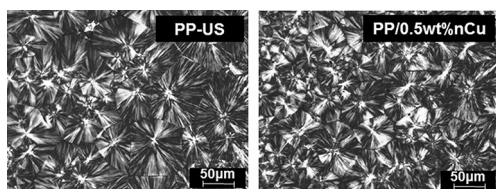

Fig. 6 Polarized optical microscopy (POM) micrographs of PP-US and PP/0.5 mass%nCu nanocomposite after the complete crystallization process at 2.5 K min^{-1}

sample presented a coarse and more imperfect macro-crystal due perhaps to their broader lamellar crystals [35], in agreement with the SAXS results.

Non-isothermal crystallization kinetics

The Jeziorny and Ozawa models have been previously used to describe the non-isothermal crystallization kinetics of polymer composites. In this work, the effect of nCu's mass percentage on the non-isothermal crystallization kinetics of polypropylene was studied in terms of both models.

The Jeziorny model has been reported by several works [14, 22, 36–41]. In this model, the non-isothermal crystallization kinetic can be described as follows:

$$1 - X_c = \exp\left(-Z_t t^n\right) \tag{1}$$

$$\log\left[-\ln\left(1 - X_c\right)\right] = n\ln t + \ln Z_t \tag{2}$$

In this model is pointed out that the value of rate parameter Z_t should be adequately corrected. Assuming constant or approximately constant the crystallization rate (ϕ), the final form of the parameter characterizing the kinetics of non-isothermal crystallization is given as follows:

$$\ln Z_c = \ln Z_t / \phi \tag{3}$$

Figure 7 displays the development of relative crystallinity as function of time for the PP-US and PP/nCu nanocomposite samples. This figure shows that the induction time and media crystallization time ($t_{0.5}$), see Table 4, of non-isothermal crystallization process of PP/nCu nanocomposites were reduced for all nanoparticles mass percentages and crystallization rates. This behavior has been reported as signal of a nucleation activity of different type of nanoparticles [15–20] in polypropylene matrices.

The non-isothermal crystallization curves obtained from the Jeziorny model are presented in Fig. 8. This figure clearly indicated a sharper transition from primary to secondary crystallization (inflection in the curve) with an increase in nCu concentration; in other words, secondary crystallization is accelerated by the nanoparticle presence, such as we previously reported for a PP/nanoclay nanocomposites [23]. Additionally, the secondary crystallization was also accelerated at low crystallization rates (2.5 K min^{-1}).

The values of n and ln Z_c determined from the slope and intercept of the initial linear portion in Fig. 8 are summarized in Table 3. It is observed in these results an effect of nanoparticles concentration specially at low crystallization rate. Firstly, the values of n decrease with the increase in mass percentages (e.g., from 3.9 for PP-US sample to 2.8 for PP/4 mass%nCu sample, at 2.5 K min^{-1}), while the Z_c values increased with the nCu mass percentages (e.g., from 0.176

Fig. 7 Development of relative crystallinity (X_c) with crystallization time (t) of PP-US and PP/nCu nanocomposites
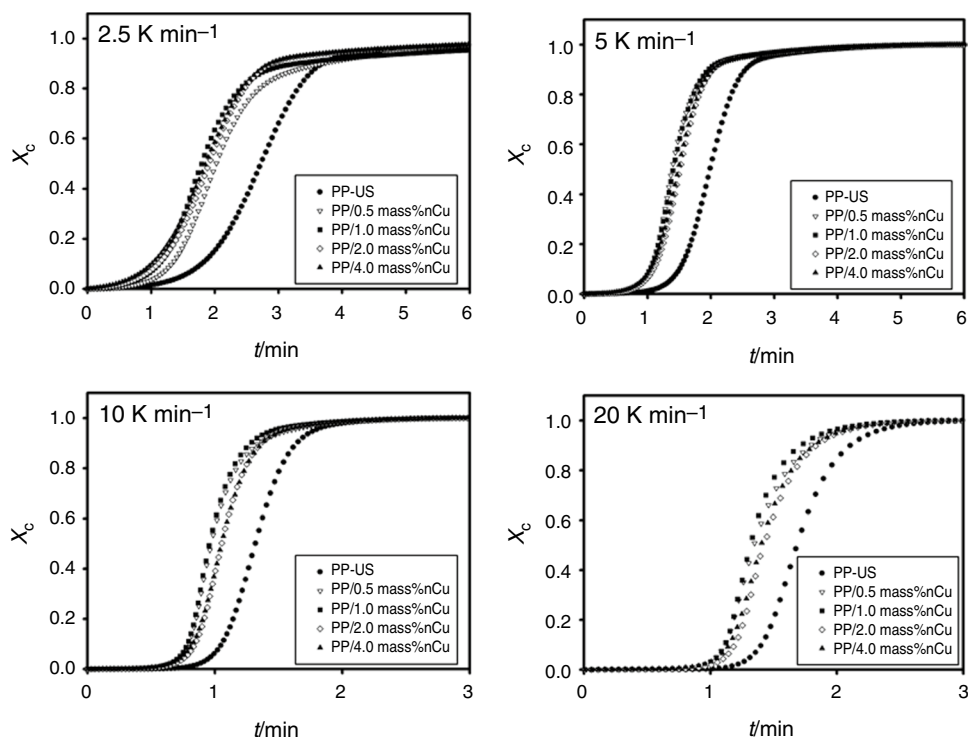
for PP-US sample to 0.425 for PP/4 mass%nCu sample, at 2.5 K min^{-1}, respectively). These results indicate a possible change in the nucleation mechanism of iPP at higher concentrations of NCu and an acceleration in the non-isothermal crystallization of iPP when it was compounded with nCu nanoparticles. In addition, the n and Z_c values increased with the crystallization rate, in agreement with some reports in the literature [28, 42]. However, the crystallization kinetic of iPP/nCu at higher crystallization rate was not adjusted by the Jeziorny approximation due to the very complicated crystallization process of polymer composites, which is much more complicated than Avrami approximation and other mathematical models, especially at higher rates, where the phenomenon of crystallization is very far from the isothermal conditions under which the Avrami model was developed [25].

On the other hand, non-isothermal crystallization kinetics of polymers has been also described through the Ozawa model [43]. This method provides information about crystal growth and the nucleation mode according to Eq. 4:

$$\ln\left[-\ln\left(1-X_c\right)\right] = \ln K(T) - m\ln\phi \quad (4)$$

where X_c is the relative crystallinity, ϕ is the cooling rate, m is the Ozawa index and $K(T)$ is the kinetic constant at temperature (T) and indicates how fast crystallization is carried out. In this theory, the non-isothermal crystallization process was considered as consisting of many infinitely small isothermal crystallization processes [37]. The

values of m and $K(T)$ function can be determined by plotting $\ln\left[-\ln\left(1-X_c\right)\right]$ versus $\ln(\phi)$ at a given temperature, and a straight line should be obtained if the non-isothermal crystallization data are adjusted to the Ozawa equation, and obtaining the slope and intercept from the straight line, respectively. The non-isothermal crystallization curves obtained from the Ozawa model for PP homopolymer and PP/nCu nanocomposites are presented in Fig. 9.

The results obtained for the Ozawa plots for the PP homopolymer and PP/nCu with the different mass percentages of nCu (0.5, 1.0, 2.0 and 4.0 mass%) show a clear two-stage crystallization process. However, the changing slope with temperature indicates that Ozawa index (m) is not constant during the crystallization process and therefore the Ozawa model cannot accurately describe non-isothermal crystallization of nanocomposites of PP loaded with copper nanoparticles. This behavior has been recently observed for composite and nanocomposites with polyolefins [36, 37, 39], and this might be attribute to that the Ozawa theory has ignored the secondary crystallization [37].

Crystallization activation energy

From the variation of crystallization peak temperature (T_p) at different cooling rates in non-isothermal crystallization process, Kissinger proposed a method to estimate the change in the activation energy (ΔE) of the crystallization process [44, 45]. However, deeper analysis has demonstrated that the Kissinger equation is mathematically inapplicable for

Fig. 8 Non-isothermal crystallization curves of PP and PP nanocomposites processed by the Jeziorny method at the different crystallization rates (2.5, 5, 10 and 20 K min⁻¹). The mass percentages of nCu were also indicated
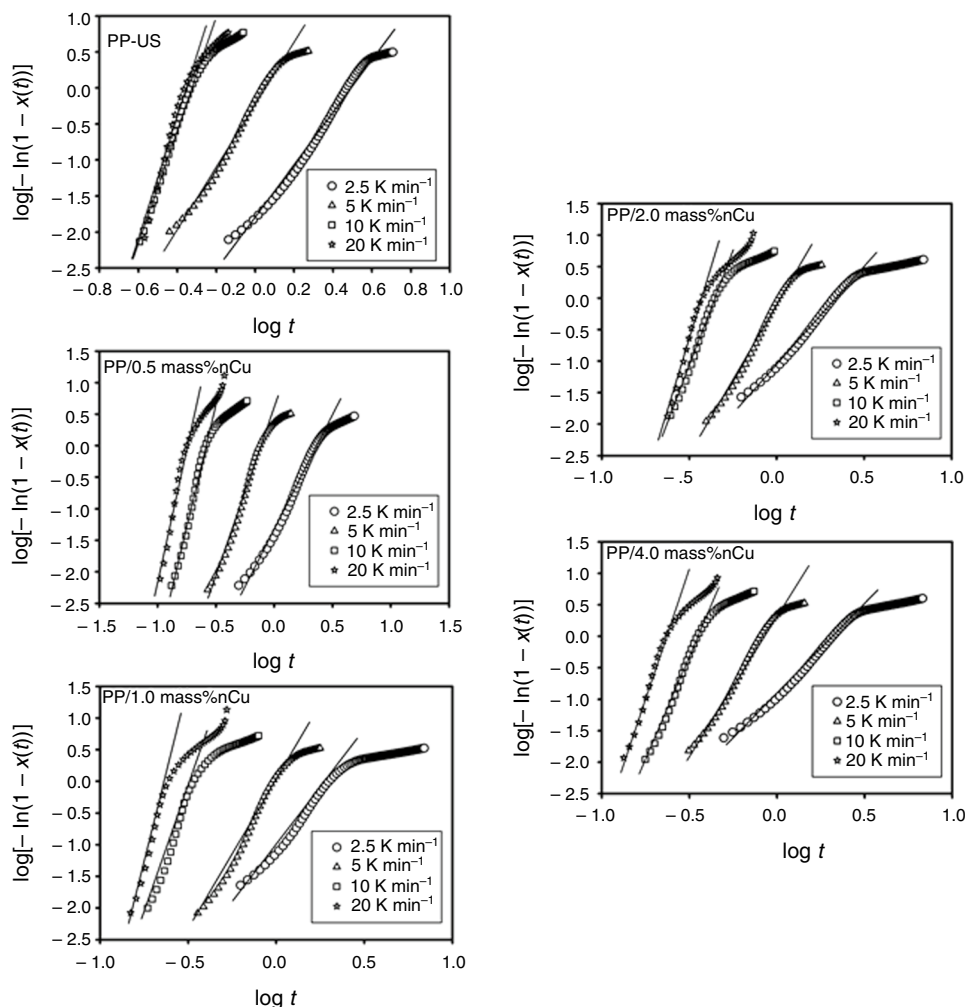
evaluations of the activation energy of processes that occur upon cooling, and for this reason the omission of negative sign in the cooling process may result in errors [46]. The correct behavior of ΔE can be determined by using isoconversional methods, such as the developed by Friedman and Vyazovkin [46]. The Friedman method [47] is valued to estimate the reliable evolution of the effective activation energy as a function of the degree of crystallinity according to Eq. 5.

$$\ln \left(\frac{\mathrm{d}X}{\mathrm{d}t} \right)_{X,\phi} = A - \frac{\Delta E_X}{RT_{X,\phi}} \tag{5}$$

where ΔE_X is the effective activation energy at a given conversion X, while $(\mathrm{d}X/\mathrm{d}t)_{X,i}$ is the instantaneous crystallization rate and $T_{X,i}$ is the set of temperatures at a given conversion X at the different cooling rates (ϕ) used. Other authors also used the isoconversional method of Friedman for obtaining results on the effective energy barrier of iPP composites [26, 48].

The dependence of the effective activation energy on the relative crystallinity for the PP and PP/nCu composites was estimated according to Eq. 4 and shown in Fig. 9 as a function of the relative crystallinity (X_c). The activation energy values calculated were negative for all samples, indicating

Table 3 Results of the kinetic analysis using the Jeziorny method for non-isothermal crystallization of PP-US and PP/nCu nanocomposites

Sample	ϕ /K min⁻¹	n	Z_t	Z_c	$t_{0.5}$	R^2
PP-US	2.5	3.9	0.013	0.176	1.42	0.9911
PP/0.5 mass%nCu		3.7	0.044	0.287	1.27	0.9864
PP/1.0 mass%nCu		3.5	0.082	0.368	1.20	0.9899
PP/2.0 mass%nCu		3.2	0.085	0.373	1.21	0.9932
PP/4.0 mass%nCu		2.8	0.118	0.425	1.19	0.9910

Fig. 9 Ozawa plots of **a** PP homopolymer (PP-US), **b** PP/nCu nanocomposite with 0.5 mass% of nCu, **c** PP/nCu nanocomposite with 1.0 mass% of nCu, **d** PP/nCu nanocomposite with 2.0 mass% of nCu and **e** PP/nCu nanocomposite with 4.0 mass% of nCu
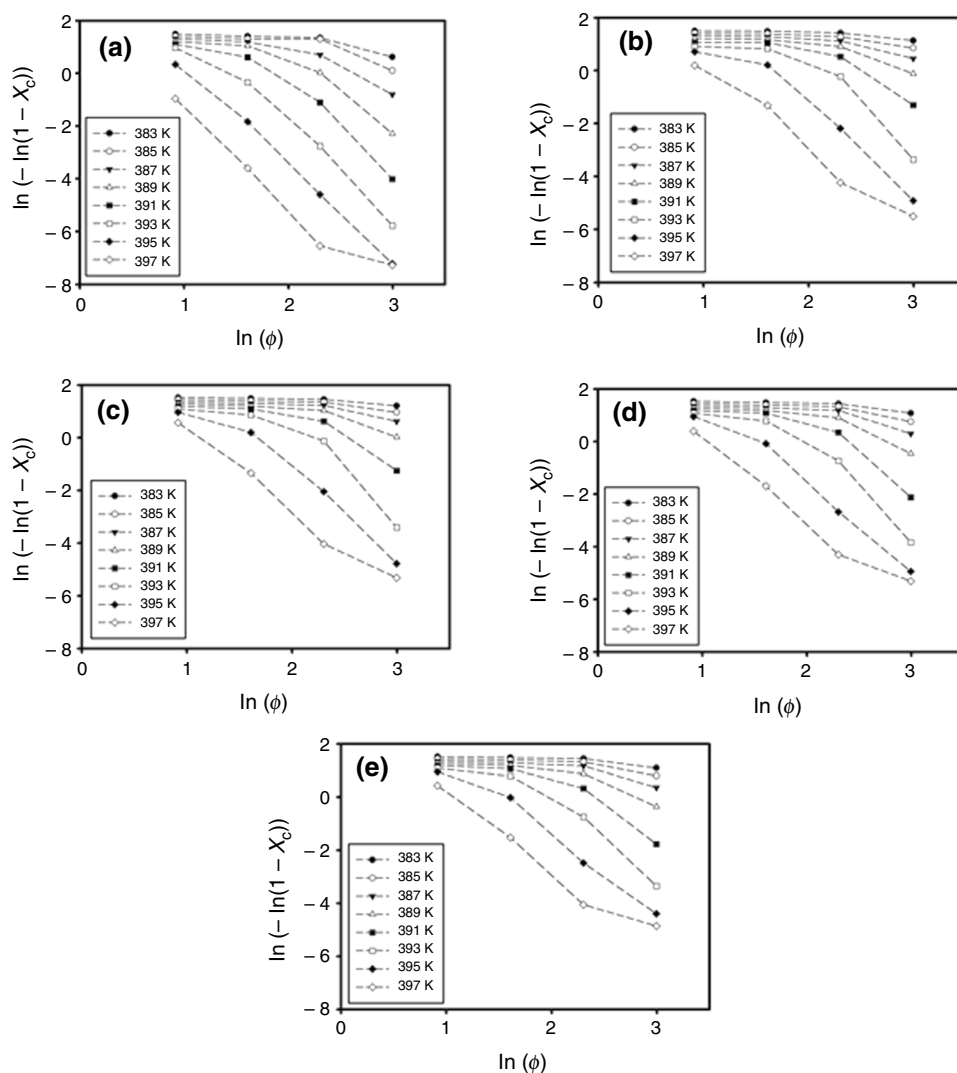
that the crystallization increases with decreasing temperature. However, the activation energy values decrease in comparison with PP-US sample when the nCu's were added at different percentages into PP matrix. This phenomenon can be ascribed to the fact that these particles could acted as nucleating agents, facilitating the crystallization of polypropylene chains. Nevertheless, energy values increase as a function of X_c for all samples due to when temperature decreases the preexisting crystallites hinder the diffusion of the macromolecular chain segments from the melt to the growth front of lamellar crystals [26, 48].

It is also shown in Fig. 10 that the final values of activation energy increase with copper amount for the PP/nCu nanocomposites filled with different concentrations of nCu (0.05, 1, 2 and 4 mass%). This behavior could be attributed to the agglomeration of Cu nanoparticles, as observed previously in Fig. 3 and Table 2, which reduces the chain mobility and thus hindering the crystallization process
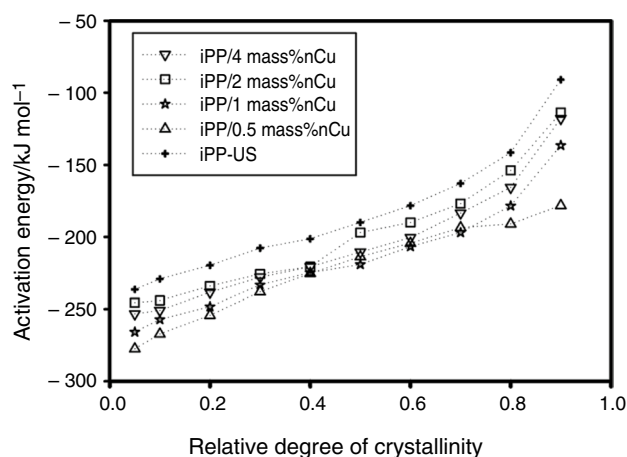

Fig. 10 Activation energy behavior as function of relative crystallinity for the neat PP and the PP/nCu nanocomposites

Table 4 Activation energy for all samples at different relative crystallinity degrees

Relative crystallinity	Activation energy/kJ mol^{-1}				
	PP-US	PP/0.5 mass%nCu	PP/1.0 mass%nCu	PP/2.0 mass%nCu	PP/4.0 mass%nCu
0.1	− 229.13	− 267.13	− 257.15	− 244.02	− 250.83
0.5	− 189.89	− 213.75	− 219.07	− 196.96	− 210.51
0.9	− 90.96	− 178.09	− 136.43	− 113.74	− 117.73

[49]. Table 4 shows the values for activation energies at various crystallinity degrees for all studied samples.

Effect of nucleation activity

The non-isothermal crystallization kinetic analysis and the crystallization activation energy results indicated a possible nucleation activity of nCu nanoparticles on the polypropylene matrix; however, it is necessary to demonstrate this behavior. The nucleation activity of different particles on the polymer matrices has been analyzed by means of Dobreva's and Gutzow method. [50].

The Dobreva and Gutzow's nucleation activity parameter of the filler is defined as:

$$\varphi = \frac{B^*}{B_0} \tag{6}$$

The parameter B can be experimentally obtained from crystallization experiences through the following relationship proposed by Dobreva and Gutzow:

$$\log \phi = \text{constant} - \frac{B}{2.3 \Delta T^2} \tag{7}$$

where ϕ is the crystallization rate, ΔT is the undercooling ($T_m - T_{\text{cpeak}}$). B^* represent the value of B when the polymer crystallizes in presence of a nucleation substrate, and B_0 when there is no nucleation agent. The value of φ can vary from 1 to 0, decreasing if the nucleation activity increases. This approach was successfully applied to evaluate nucleating rate differences of iPP containing different mineral fillers [18, 20, 28].

In Fig. 11, Dobreva analysis results are presented for the PP-US sample and the PP/nCu nanocomposites. The nucleation activity can be calculated by the ratio between the slopes of linear curves of log ϕ versus $1/(2.3\Delta T^2)$. The results of B_0, B^* and φ are presented in Table 5. It is clearly observed, from these results, that the values of φ for the PP-US sample did not decrease with the incorporation of nCu's, indicating that this type of nanoparticles did not act as nucleating agent of iPP matrix, unlike those reported for other types of nanoparticles [26, 28, 42].

Additionally, from the definition of B, it is possible to determine the polymer crystal surface energy (σ), which is related to the necessary energy to crystallize a macromolecular segment and can be estimated by Eq. 7:

$$B = \frac{16\pi\sigma^3 V_m^2}{3kT_m \Delta S_m^2 n} \tag{8}$$

where σ is the crystal surface energy, the PP molar volume (V_m) can be taken equal to 28 cm^3 mol^{-1}, k is the Boltzmann Constant, T_m is the PP melting temperature, the molar entropy (ΔS_m) 24.2 J K^{-1}, the Avrami exponent $n = 3$. The values of σ for all studied samples are reported in Table 5. According to these results, the incorporation of nCu did not significantly modified the crystal surface energy, corroborating the no nucleating activity of these nanoparticles.

Effect of thermal conductivity

After the previous results, it is necessary to make next question, what could be the reason for the acceleration of non-isothermal crystallization kinetic and the reduction in the activation energy kinetic, if the nCu's did not show a conventional nucleation activity? In this sense is necessary to state that from to the literature, the copper nanoparticles have low specific heat capacity ($C_p \approx 0.39$ J kg^{-1} K^{-1}) and high thermal conductivity ($\kappa \approx 386$ W m^{-1} K^{-1}). These properties
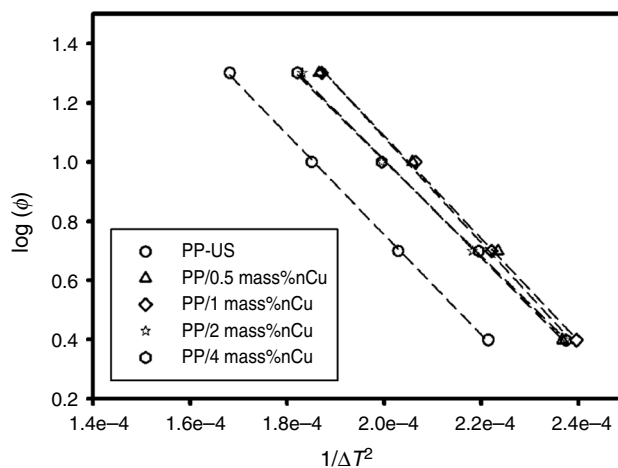

Fig. 11 Dobreva's graphs of PP-US and PP/nCu nanocomposite samples

Table 5 Nucleation activity parameters and crystal surface energy of PP-US and PP/nCu nanocomposite samples

Sample	A	B_0	$B*$	$\varphi(B*/B_0)$	R^2	Crystal surface energy σ/J cm^{-2}
PP-US	4.146	39,049.67	–	–	0.9996	2.27E−06
PP/0.5 mass%nCu	4.649	–	41,053.28	1.05	0.9935	2.31E−06
PP/1.0 mass%nCu	4.562	–	39,982.38	1.02	0.9985	2.29E−06
PP/2.0 mass%nCu	4.318	–	38,126.86	0.98	0.9987	2.25E−06
PP/4.0 mass%nCu	4.242	–	39,116.45	1.00	0.9993	2.27E−06

could help to obtain PP/nCu nanocomposites with higher thermal conductivity than the neat PP. In this case, the measured k was 0.23, 72.4, 78.4, 76.3 W m^{-1} K^{-1} for the PP/nCu nanocomposites containing 0.5, 1.0, 2.0 and 4.0 mass% of copper nanoparticles. These results indicate a significant increasing respect to the literature reported of k for iPP (0.11 W m^{-1} K^{-1}) [51]. These values of k could be related to materials with high heat dissipation properties. Therefore, a possible explanation to the acceleration in the crystallization kinetic and the activation energy behavior of PP/nCu nanocomposites could be related to an increase in the thermal energy dissipation from the melted iPP macromolecules to the individual or agglomerated nanoparticles and then to the surroundings during the non-isothermal crystallization. This behavior was previously reported by Radhakrishnan et al. [29, 30], who studied the effect of thermal conductivity and heat transfer of different fillers (wollastonite, glass fiber, silica, talc, mica, calcium carbonate and carbon fiber) on the crystallization, structure and morphology of polypropylene experimentally and by a phenomenological model. These authors found that higher thermal conductivity of the filler promotes to shorter induction time and faster crystallization due to the thermal dissipation from the melt to the surroundings in a molding (injection or compression) process. Conversely, although there are evidences on the effect of high thermal conductivity fillers on the overall crystallization process of polypropylene, it is necessary to develop further studies on this phenomenon and determine if the high thermal conductivity nanoparticles affected the crystallization of semicrystalline polymers at molecular (secondary nucleation) or bulk level.

Conclusions

The non-isothermal crystallization kinetic, crystalline morphology and crystallization activation energy of iPP/nCu nanocomposites under different concentrations of nanoparticles (i.e., 0.1, 0.5, 1.0, 2.0 and 4.0 mass%) and different crystallization rates (2.5, 5.0, 10.0 and 20.0 K min^{-1}) were investigated. The nucleation activity in terms of Dobreva and Gutzow method and thermal conductivity measurements were performed to determine if the crystallization behavior

was due to a nucleating effect of nanoparticles on the iPP matrix or if the high thermal conductivity of nanoparticles favored the thermal dissipation.

The results indicate that incorporation of nCu increased the T_p of crystallization about 4 K respect to the neat PP and reduce the induction time and $t_{0.5}$ of crystallization. Additionally, the crystallization kinetics, according to Jeziorny analysis at low crystallization rate (2.5 K min^{-1}), was also accelerated, and the activation energy was reduced for all PP/nCu nanocomposites.

Although this behavior has been previously attributed to a heterogeneous nucleating effect of nanoparticles on the iPP matrix, the nucleation activity of nCu, obtained by the Dobreva and Gutzow method, was practically insignificant. Similarly, the crystal surface energy of iPP was not influenced by the nCu's.

Conversely, the PP/nCu nanocomposites presented high thermal conductivity, which helped to dissipate better the thermal energy released during the crystallization process. Therefore, there are evidences that the observed non-isothermal crystallization behavior (Kinetic and activation energy) was more influenced by the high thermal conductivity of nanocomposites than for the conventional nucleation activity of nanoparticles.

References

1. Móczó J, Pukánszky B. Polymer micro and nanocomposites: structure, interactions, properties. J Ind Eng Chem. 2008;14:535–63.
2. Zhang S, Cao XY, Ma YM, Ke YC, Zhang JK, Wang FS. The effects of particle size and content on the thermal conductivity and mechanical properties of Al$_2$O$_3$/high density polyethylene (HDPE) composites. Express Polym Lett. 2011;5:581–90.
3. Kratochvíla J, Boudenne A, Krupa I. Effect of filler size on thermophysical and electrical behavior of nanocomposites based on

expanded graphite nanoparticles filled in low-density polyethylene matrix. Polym Compos. 2013;34:149–55.

4. Masirek R, Szkudlarek E, Piorkowska E, Slouf M, Kratochvil J, Baldrian J. Nucleation of isotactic polypropylene crystallization by gold nanoparticles. J Polym Sci Part B Polym Phys. 2010;48:469–78.

5. Isayev AI, Kumar R, Lewis TM. Ultrasound assisted twin screw extrusion of polymer–nanocomposites containing carbon nanotubes. Polymer. 2009;50:250–60.

6. Yang L, Zhang Z, Wang X, Chen J, Li H. Effect of ultrasonic irradiation on the microstructure and the electric property of PP/CPP/MWNT composites. J Appl Polym Sci. 2012;128:1510–20.

7. Ávila-Orta CA, Martínez-Colunga JG, Bueno-Baqués D, Raudry-López CE, Cruz-Delgado VJ, González-Morones P, Valdéz-Garza JA, Esparza-Juárez ME, Espinoza-González CJ, Rodríguez-González JA. Proceso continuo asistido por ultrasonido de frecuencia y amplitud variable, para la preparación de nanocompuestos a base de polímeros y nanopartículas. Mx. Patent MX/a/2009/003842, 19 September 2014.

8. Mata-Padilla JM, Ávila-Orta CA, Medellín-Rodríguez FJ, Hernández-Hernández E, Jiménez-Barrera RM, Crúz-Delgado VJ, et al. Structural and morphological studies on the deformation behavior of polypropylene/multi-walled carbon nanotubes nanocomposites prepared through ultrasound-assisted melt extrusion process. J Polym Sci Part B Polym Phys. 2015;53:475–91.

9. Ávila-Orta C, Quiñones-Jurado Z, Waldo-Mendoza M, Rivera-Paz E, Cruz-Delgado V, Mata-Padilla J, et al. Ultrasound-assist extrusion methods for the fabrication of polymer nanocomposites based on polypropylene/multi-wall carbon nanotubes. Materials (Basel). 2015;8:7900–12.

10. Suktha P, Lekpet K, Siwayaprahm P, Sawangphruk M. Enhanced mechanical properties and bactericidal activity of polypropylene nanocomposite with dual-function silica-silver core–shell nanoparticles. J Appl Polym Sci. 2013;128:4339–45.

11. Tjong SC, Bao S. Structure and mechanical behavior of isotactic polypropylene composites filled with silver nanoparticles. E-Polymers. 2007. https://doi.org/10.1515/epoly.2007.7.1.1618.

12. Dehnavi MH, Asghar A, Jeddi A, Gharehaghaji AA, Yazdanshenas ME. Thermal properties of conductive nanocomposite core–shell filament yarns. Indian J Fibre Text Res. 2013;38:380–6.

13. Fredin L, Li Z, Lanagan MT, Ratner M, Marks TJ. Substantial recoverable energy storage in percolative metallic aluminum-polypropylene nanocomposites. Adv Funct Mater. 2013;23:3560–9.

14. Delgado K, Quijada R, Palma R, Palza H. Polypropylene with embedded copper metal or copper oxide nanoparticles as a novel plastic antimicrobial agent. Lett Appl Microbiol. 2011;53:50–4.

15. España-Sánchez BL, Ávila-Orta CA, Padilla-Vaca F, Neira-Velázquez MG, González-Morones P, Rodríguez-González JA, et al. Enhanced antibacterial activity of melt processed poly(propylene) Ag and Cu nanocomposites by argon plasma treatment. Plasma Process Polym. 2014;11:353–65.

16. Gawish SM, Avci H, Ramadan AM, Mosleh S, Monticello R, Breidt F, et al. Properties of antibacterial polypropylene/nanometal composite fibers. J Biomater Sci Polym. 2012;23:43–61.

17. Arranz-Andrés J, Pérez E, Cerrada M. Nanocomposites based on isotactic polypropylene–copper nanoparticles as electromagnetic shields. Sci Adv Mater. 2013;5:1524–32.

18. Cruz-Delgado VJ, Ávila-Orta CA, Espinoza-Martínez AB, Mata-Padilla JM, Solis-Rosales SG, Jalbout AF, et al. Carbon nanotube surface-induced crystallization of polyethylene terephthalate (PET). Polymer. 2014;55:642–50.

19. Mikešová J, Šlouf M, Gohs U, Popelková D, Vacková T, Vu NH, et al. Nanocomposites of polypropylene/titanate nanotubes: morphology, nucleation effects of nanoparticles and properties. Polym Bull. 2014;71:795–818.

20. Espinoza-Martínez AB, Ávila-Orta CA, Cruz-Delgado VJ, Medellín-Rodríguez FJ, Bueno-Baqués D, Mata-Padilla JM. Effect of MWNTs concentration and cooling rate on the morphological, structural, and electrical properties of non-isothermally crystallized PEN/MWNT nanocomposites. J Appl Polym Sci. 2015;132:1–8.

21. Espinoza-Martinez AB, Avalos-Belmontes F, De Valle LFR, Espinoza-Martinez PA, Avila-Orta CA, Soriano-Corral F, et al. Morphological study and dielectric behavior of nonisothermally crystallized poly(ethylene naphthalate) nanocomposites as a function of graphene content. J Nanomater. 2016;2016:9846102.

22. Jeziorny A. Parameters characterizing the kinetics of the non-isothermal crystallization of poly(ethylene terephthalate) determined by DSC. Polymer. 1978;19:1142–4.

23. Medellín-Rodríguez FJ, Mata-Padilla JM, Hsiao BS, Waldo-Mendoza MA, Ramírez-Vargas E, Sánchez-Valdes S. The effect of nanoclays on the nucleation, crystallization, and melting mechanisms of isotactic polypropylene. Polym Eng Sci. 2007;47:1889–97.

24. Chae DW, Kim BC. Physical properties of isotactic poly(propylene)/silver nanocomposites: dynamic crystallization behavior and resultant morphology. Macromol Mater Eng. 2005;290:1149–56.

25. Du M, Guo B, Wan J, Zou Q, Jia D. Effects of halloysite nanotubes on kinetics and activation energy of non-isothermal crystallization of polypropylene. J Polym Res. 2010;17:109–18.

26. Hao W, Li W, Yang W, Shen L. Effect of silicon nitride nanoparticles on the crystallization behavior of polypropylene. Polym Test. 2011;30:527–33.

27. Alvarez VA, Perez CJ. Effect of different inorganic filler over isothermal and non-isothermal crystallization of polypropylene homopolymer. J Therm Anal Calorim. 2012;107:633–43.

28. Ferreira CI, Dal Castel C, Oviedo MAS, Mauler RS. Isothermal and non-isothermal crystallization kinetics of polypropylene/exfoliated graphite nanocomposites. Thermochim Acta. 2013;553:40–8.

29. Radhakrishnan S, Sonawane PS. Role of heat transfer and thermal conductivity in the crystallization behavior of polypropylene-containing additives: a phenomenological model. J Appl Polym Sci. 2003;89:2994–9.

30. Radhakrishnan S, Sonawane P, Pawaskar N. Effect of thermal conductivity and heat transfer on crystallization, structure, and morphology of polypropylene containing different fillers. J Appl Polym Sci. 2004;93:615–23.

31. Hwang H, Lee KY, Yeo T, Choi W. Investigation of structural and chemical transitions in copper oxide microstructures produced by combustion waves in a mixture of CuO–Cu₂O–Cu and fuel. Appl Surf Sci. 2015;359:931–8.

32. Hybiak D, Garbarczyk J. Silver nanoparticles in isotactic polypropylene (iPP)* Part I. Silver nanoparticles as metallic nucleating agents for β-iPP polymorph. Polymers. 2014;59:585–91.

33. Slouf M, Vacková T, Zhigunov A, Sikora A, Piorkowska E. Nucleation of polypropylene crystallization with gold nanoparticles. Part 2: relation between particle morphology and nucleation activity. J Macromol Sci Part B. 2016;55:393–410.

34. Fanegas N, Gámez MA, Marco C, Jiménez I, Ellis G. Influence of a nucleating agent on the crystallization behaviour of isotactic polypropylene and elastomer blends. Polymer. 2007;48:5324–31.

35. Medellín-Rodríguez FJ, Mata-Padilla M, Sánchez-Valdes S, Vega-Díaz S, Dávalos-Montoya O. Step-like melting mechanisms of isothermally crystallized isotactic polypropylene. J Polym Sci Part B Polym Phys. 2008;46:2188–200.

36. Coburn N, Douglas P, Kaya D, Gupta J, McNally T. Isothermal and non-isothermal crystallization kinetics of composites of poly(propylene) and MWCNTs. Adv Ind Eng Polym Res. 2018;1:99–110.

37. Lu Y, Tang Y, Xia X. Non-isothermal crystallization of copper-containing composite based on polymer alloy of poly(ethylene oxide) and polyethylene. Thermochim Acta. 2018;670:61–70.

38. Chen Y, Yin Q, Zhang X, Xue X, Jia H. The crystallization behaviors and rheological properties of polypropylene/graphene nanocomposites: the role of surface structure of reduced graphene oxide. Thermochim Acta. 2018;661:124–36.

39. Rasana N, Jayanarayanan K, Pegoretti A. Non-isothermal crystallization kinetics of polypropylene/short glass fibre/multiwalled carbon nanotube composites. RSC Adv. 2018;8:39127–39.

40. Layachi A, Makhlouf A, Frihi D, Satha H, Belaadi A, Seguela R. Non-isothermal crystallization kinetics and nucleation behavior of isotactic polypropylene composites with micro-talc. J Therm Anal Calorim. 2019;138:1081–95.

41. Wu Z, Zhang Z, Mai K. Non-isothermal crystallization kinetics of UHMWPE composites filled by oligomer modified $CaCO_3$. J Therm Anal Calorim. 2020;139:1111–20.

42. Ardanuy M, Velasco JI, Realinho V, Arencón D, Martínez AB. Non-isothermal crystallization kinetics and activity of filler in polypropylene/Mg–Al layered double hydroxide nanocomposites. Thermochim Acta. 2008;479:45–52.

43. Ozawa T. Kinetics of non-isothermal crystallization. Polymer. 1971;12:150–8.

44. Kissinger HE. Variation of peak temperature with heating rate in differential thermal analysis. J Res Natl Bur Stand. 1934;1956(57):217.

45. Blaine RL, Kissinger HE. Homer Kissinger and the Kissinger equation. Thermochim Acta. 2012;540:1–6.

46. Vyazovkin S. Is the Kissinger equation applicable to the processes that occur on cooling? Macromol Rapid Commun. 2002;23:771–5.

47. Friedman HL. Kinetics of thermal degradation of char-forming plastics from thermogravimetry. Application to a phenolic plastic. J Polym Sci Part C Polym Symp. 2007;6:183–95.

48. Gonzalez-Calderon J, Castrejon-Gonzalez EO, Medellin-Rodriguez FJ, Stribeck N, Almendarez-Camarillo A. Functionalization of multi-walled carbon nanotubes (MWCNTs) with pimelic acid molecules: effect of linkage on β-crystal formation in an isotactic polypropylene (iPP) matrix. J Mater Sci. 2015;50:1457–68.

49. Ma W, Wang X, Zhang J. Crystallization kinetics of poly (vinylidene fluoride)/MMT, SiO_2, $CaCO_3$, or PTFE nanocomposite by differential scanning calorimeter. J Therm Anal Calorim. 2011;103:319–27.

50. Dobreva A, Gutzow I. Activity of substrates in the catalyzed nucleation of glass-forming melts. II. Experimental evidence. J Non Cryst Solids. 1993;162:13–25.

51. Han Z, Fina A. Thermal conductivity of carbon nanotubes and their polymer nanocomposites: a review. Prog Polym Sci. 2011;36:914–44.